Magnetism and anisotropy of ultrathin Ni films on Cu(001)

J. Henk, A. M. N. Niklasson, and B. Johansson
Condensed Matter Theory Group, Physics Department, University Uppsala, S-751 21 Uppsala, Sweden
(Received 3 September 1998; revised manuscript received 10 November 1998)

Both magnetic structure and magnetic-anisotropy energies are calculated for cubic and tetragonal Ni films on Cu(001) for thicknesses from 1 to 10 monolayers. The magnetic reorientation transition from in-plane to perpendicular anisotropy can be attributed to the volume contribution in tetragonal films which is discussed in terms of layer-resolved band energies. The transition takes place at six to seven monolayers, in agreement with experiments. The layer-dependent magnetic properties are brought into relation to those at a Ni(001) surface and a Ni(001)/Cu(001) interface, thus allowing the identification of contributions which are due to quantum-size effects. For films of a few monolayer thickness, the effect of quantized electronic states on the anisotropy appears to be significant. [S0163-1829(99)05613-1]

I. INTRODUCTION

Ultrathin Ni films grown on Cu(001) show a peculiar behavior regarding the magnetic anisotropy: at film thicknesses between 5 monolayers (ML) and 7 ML—depending on film preparation and temperature—a sharp spin reorientation transition (SRT) from in-plane to perpendicular magnetization is observed experimentally. At much higher thickness, in the range from about 35 ML to 70 ML, the magnetic moments reorientate gradually and become again parallel to the surface.[1–4] This remarkable finding is contrary to those for Fe or Co films grown on Cu(001): the first show a SRT from perpendicular to in-plane anisotropy at about 5 ML; the latter show in-plane anisotropy for all thicknesses and thus no SRT [this has attracted a lot of attention and among a vast literature we refer to Refs. 5–9 for Fe/Cu(001) and Refs. 10–13 for Co/Cu(001)].

Ni films grow epitaxially on Cu(001), but due to the lattice mismatch between Ni(001) and Cu(001), the films become tetragonally distorted on Cu(001). The first SRT can be understood by the magnetoelastic anisotropy due to this tetragonal distortion of the Ni films—as has been shown experimentally by Farle *et al.*[14] and theoretically by Hjortstam *et al.*[15] for hypothetical fct-bulk Ni, thus focusing on the volume contribution to the magnetic-anisotropy energy (MAE). However, from calculations for bulk materials with different c/a ratios it is hardly possible to conclude at which particular film thickness a SRT will occur. For example, bulk calculations cannot address the quantization of electronic states within the Ni film which may affect the MAE considerably, in particular for very thin films. Further, the anisotropy at both the surface and the Ni/Cu interface may affect the MAE—and thus the transition thickness—substantially. Therefore, calculations for ultrathin Ni films which take into account the correct boundary conditions as well as the film relaxation are absolutely necessary in order to explain the first SRT.

The second (gradual) SRT can be understood by the formation of films with misfit dislocations which occur due to strain relaxation, as has been observed experimentally.[3,4] The latter lowers the MAE and thus causes the magnetization to switch back from perpendicular to in-plane anisotropy. Further, island growth has been reported[16] which makes it difficult—if not impossible—to conclude from theory on the second SRT.

Ni films with thickness of a few or more ML can be regarded as composed by a Ni(001)/Cu(001) interface and a Ni(001) surface. These two contributions to the magnetic moments and the MAE should be easy to identify. However, the quantization of electronic states within the film should also influence these quantities, in particular for very thin films where the above decomposition into surface and interface should become at least questionable. Sophisticated calculations of the magnetization profiles (layer-dependent magnetic moments) or the MAE are very time consuming. Therefore, it appears desirable—for both theoreticians and experimentalists—to be able to derive reliable quantitative results from a knowledge of only the magnetization profiles or anisotropy energies of the interface and the surface, constructing from these the profile for the entire film. In this procedure, one neglects, however, the quantum-well contribution.

In this paper, we report on calculations of both the magnetic structure and the MAE of cubic as well as tetragonally distorted Ni films on Cu(001) for thicknesses from 1 ML up to 10 ML. In Sec. II we provide the reader with definitions, address our theoretical approach, and discuss the ingredients used in the numerical calculations. In Sec. III we consider the superposition of magnetization and band-energy profiles in order to understand better our results. The latter will be discussed in Sec. IV, in particular the magnetization profiles (Sec. IV A) and the magnetic anisotropy (Sec. IV B). Conclusions are given in Sec. V.

II. THEORETICAL AND COMPUTATIONAL ASPECTS

Our procedure to calculate the MAE is based on two steps. First, the scalar-relativistic linear muffin-tin orbital (LMTO) method is applied for the generation of self-consistent spin-dependent potentials of the semi-infinite system consisting of substrate layers, ferromagnetic film layers, and vacuum, thus ignoring at this step spin-orbit coupling (SOC). Second, fully relativistic layer Korringa-Kohn-Rostoker (LKKR) calculations yield the layer-resolved Bloch spectral functions, from which the MAE is calculated. Here, magnetic exchange and the SOC are treated on equal footing. This scheme is not self-consistent and therefore re-

lies on a good approximation of the potentials. On the other hand, the SOC is not treated as a perturbation.

The Green function (GF) technique of the LMTO method[17,18] was developed by Skriver and Rosengaard[19] and is used in the calculation of the self-consistent potentials in the tight-binding,[20] frozen-core, and atomic-sphere approximations in conjunction with the local spin-density approximation as parametrized by Vosko, Wilk, and Nusair.[21] It does not rely on a slab or supercell geometry. Thus, a correct description of the loss of translational symmetry perpendicular to the surface—as is present in semi-infinite systems—is ensured. Furthermore, the principle-layer technique[22] leads to minimal computational effort which scales linearly with the number of layers taken into account. The results of this first step are spin- and layer-dependent muffin-tin potentials (the Wigner-Seitz radius is 2.669 a.u.) which are used as input for the LKKR calculations.

The method used in the calculation of the LKKR Green function should also be sketched.[23] The layer-diagonal part G_{ll} is obtained by first calculating the GF of an empty layer, i.e., a layer with zero potential, embedded in the host system and taking into account the correct boundary conditions (reflection at the surface side and at the bulk side of the empty layer). Then the Dyson equation for this empty layer is solved, giving the $\vec{k}_\parallel$- and energy-resolved scattering-path operator.[24] Because only matrices related to single layers are involved in this computational scheme, the computing time scales linearly with the number of layers, without using any screened representation (''tight binding''). The layer-nondiagonal parts $G_{ll'}$ (not used in this paper, though) can by obtained from G_{ll} and the multiple-scattering transfer matrices from layer l to layer l'. Details of this method will be published elsewhere.

The LKKR calculations were performed for two collinear magnetic configurations: $\vec{M}^{(\parallel)}$ with all local magnetic moments aligned parallel to the layers and $\vec{M}^{(\perp)}$ with all local magnetic moments aligned perpendicular to the layers (parallel to the surface normal). We applied the so-called force theorem; i.e., both calculations used the same potentials. The layer-dependent electronic structure for a magnetic configuration $\vec{M}$ is conveniently discussed in terms of the Bloch spectral function $D^{(l)}$,

$$D^{(l)}(\vec{k}_\parallel, E; \vec{M}) = \frac{1}{\pi} \lim_{\eta \to 0_+} \mathrm{Im}\,\mathrm{Tr}\, G_{ll}(\vec{k}_\parallel, E - \mathrm{i}\eta; \vec{M}), \quad (1)$$

which for layer l, energy E, and surface-parallel wave vector $\vec{k}_\parallel$ is calculated from the layer-diagonal part of the GF, $G_{ll}(\vec{k}_\parallel, E - \mathrm{i}\eta; \vec{M})$, $\eta > 0$. The layer-density of states (LDOS) is obtained from $D^{(l)}$ by integration over the surface Brillouin zone (SBZ),

$$N^{(l)}(E; \vec{M}) = \int_{\mathrm{SBZ}} D^{(l)}(\vec{k}_\parallel, E; \vec{M})\, d\vec{k}_\parallel . \quad (2)$$

For the above integration we generated special-point sets by the Monkhorst-Pack method for two-dimensional lattices.[25,26] Although in the case of perpendicular magnetization the point group is C_4 (in Schönflies notation), we used the $\vec{k}_\parallel$ mesh for the point group C_s—which is the relevant one in the case of in-plane magnetization—in order to avoid any inconsistencies. Convergence was checked for sets from 120 points with up to 1830 points. For films thicker than about 5 ML we found convergence for point sets with 600–$800\vec{k}_\parallel$. Thin films, in particular 1 ML and 2 ML, showed rather slow convergence. The results of the calculations presented here were obtained with a 1275 point set. Note that the number of k-points is rather small compared to that used in calculations of the bulk MAE.[27,28] But due to the calculation of the layer-resolved GF of a semi-infinite system, the integration over $k_\perp$ is in principle included (although it is not performed explicitly due to the computational scheme for the GF), and we thus use—roughly speaking—a sampling over symmetry-adapted $\vec{k}$ directions.

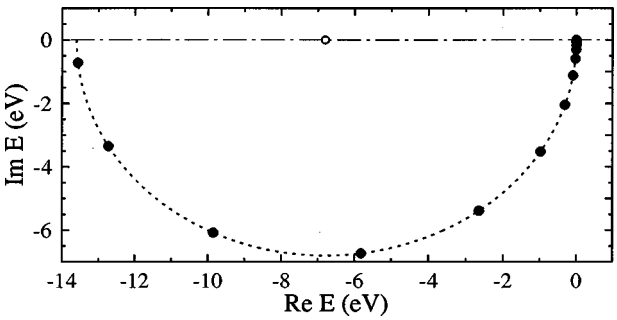

FIG. 1. Contour and mesh used in the complex energy integration. Solid circles represent points on a logarithmic angular mesh; cf. Eq. (6). The open circle is the center of the semicircle contour with radius 0.5 Ry; the Fermi energy is at 0 eV.

The band energy $E^{(l)}_{\mathrm{bnd}}$ of layer l is given by

$$E^{(l)}_{\mathrm{bnd}}(\vec{M}) = \int_{-\infty}^{E_\mathrm{F}} (E - E_\mathrm{F}) N^{(l)}(E; \vec{M})\, dE, \quad (3)$$

with E_F denoting the Fermi energy. The total band energy of a system with n ferromagnetic layers on a nonmagnetic substrate, in brief $\mathrm{Ni}_n/\mathrm{Cu}(001)$, is then simply a sum over all magnetic layers,

$$E_{\mathrm{bnd}}(\vec{M}) = \sum_{l=1}^{n} E^{(l)}_{\mathrm{bnd}}(\vec{M}). \quad (4)$$

Note that in principle the magnetic film (Ni) induces magnetic moments in the substrate layers (Cu) at the interface. This can be accounted for by extending the above sum, Eq. (4), over all energetically perturbed layers. For the energy integration in Eq. (3) we exploit the analytical properties of the GF and replace the integral along the real energy axis by a contour integration. Because E_{bnd} of the core levels are expected not to depend significantly on the magnetization direction, we take into account only the valence-band regime (frozen-core approximation). As contour we chose a semicircle with radius R and center $E_\mathrm{F} - R$ (see Fig. 1). The applied Gaussian quadrature with 16 sampling points on an angular logarithmic mesh appeared to be very accurate and robust, and has the advantage that sampling on the real axis is avoided. The sampling points z_j are given by

$$z_j = E_\mathrm{F} + R[\exp(i\vartheta_j) - 1], \quad j = 1, \ldots, 16, \quad (5)$$

with angles ϑ_j on a logarithmic mesh in $[-\pi, 0]$,

$$\vartheta_j = -\pi \frac{\exp(\beta) - \exp(\beta x_j)}{\exp(\beta) - \exp(-\beta)}, \quad j = 1, \ldots, 16, \tag{6}$$

and $x_j \in]-1,1[$, $j = 1, \ldots, 16$, are the zeros of the respective Legendre polynomial used in the Gaussian quadrature.[29] The density of the sampling points near the Fermi energy is controlled by $\beta > 0$. The radius R is chosen in such a way that the whole valence-band regime is covered. In the calculations presented below we chose $\beta = -3.222\,32$ and $R = 0.5$ Ry.

The magnetic-anisotropy energy E_{MA} is finally given by the differences of the band energies and the dipole-dipole interaction energies $E_{\mathrm{dd}}(\vec{M})$ for in-plane ($\vec{M}^{(\parallel)}$) and perpendicular magnetization ($\vec{M}^{(\perp)}$),

$$E_{\mathrm{MA}} = E_{\mathrm{bnd}}(\vec{M}^{(\parallel)}) + E_{\mathrm{dd}}(\vec{M}^{(\parallel)}) - E_{\mathrm{bnd}}(\vec{M}^{(\perp)}) - E_{\mathrm{dd}}(\vec{M}^{(\perp)}). \tag{7}$$

We used the Ewald summation technique as outlined in Ref. 30 for the calculation of $E_{\mathrm{dd}}(\vec{M})$.

In order to check the numerical accuracy, the band energies were calculated for $\vec{M} \| [001]$ and $\vec{M} \| [010]$ for semi-infinite Ni(001) (in the Cu lattice). We found an energy difference less than 0.4 μeV for bulklike layers ($l = 10$). Note that in the bulk the above difference should be zero. As will be seen below, the above value is about two to three orders of magnitude smaller than the MAE in thin films.

The Ni layers are assumed to continue epitaxially the Cu fcc lattice in the [001] direction. We distinguish three cases of relaxations in the Ni films. (i) In the ''fcc case,'' the interlayer distance is that of bulk Cu, (ii) In the ''fct case,'' the interlayer distance is reduced by 6.9% in order to retain the volume of the bulk-Ni unit cell. (iii) Using low-energy electron diffraction (LEED), Müller *et al.*, obtained experimentally the interlayer distances for 3-ML, 5-ML, and 11-ML films[31] which we refer to as the ''fct LEED'' case. In all three cases, we use the in-plane lattice constant of bulk Cu, i.e., a next-nearest neighbor distance of 2.55 Å. A theoretical LEED analysis on Cu(001), however, found best agreement with experimental data with a slightly reduced in-plane lattice constant (0.8%), indicating strain even at uncovered Cu(001) surfaces.[32] For convenience, we denote the surface layer by S, the second layer by $S-1$, etc.

III. SUPERPOSITION OF MAGNETIZATION AND BAND-ENERGY PROFILES

In the following, we show that magnetization and band-energy profiles of Ni/Cu films can essentially be regarded as superimposed by profiles which originate from two independent perturbations at the two boundaries of the film, i.e., the Ni/Cu interface and the Ni surface.[33]

We describe unperturbed bulk Ni by a spin-dependent nonrelativistic Green function G_B^σ, $\sigma = \pm$ being the spin index. We construct a Ni film on a Cu substrate by replacing an infinite Ni crystal [bulk (B)] by Cu (R) on the right-hand side and by vacuum (L) on the left-hand side of the Ni layers which constitute the film (cf. Fig. 2). The film layers are then influenced by spin-dependent perturbations V_L^σ and V_R^σ, at the two boundaries. The film GF G^σ thus has to fulfill the

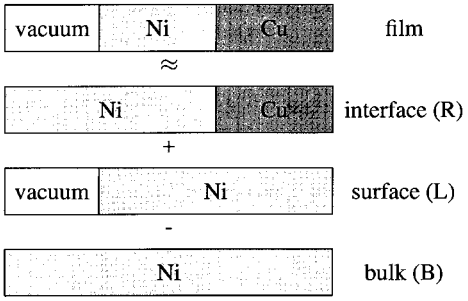

FIG. 2. Schematic construction of a Ni film on Cu (top). Starting from Ni bulk (bottom, light grey), two semi-infinite solids are replaced by vacuum (white) and by Cu (dark grey), yielding the surface (L) and the interface (R) system, respectively. For letters B, L, and R see Sec. III. The mathematical signs ($\approx$, $+$, $-$) refer to Eqs. (9) and (14).

Dyson equation $G^\sigma = G_B^\sigma + G_B^\sigma (V_L^\sigma + V_R^\sigma) G^\sigma$. Its series expansion can be written as

$$G^\sigma = \sum_{j=0}^{\infty} G_B^\sigma [(V_L^\sigma + V_R^\sigma) G_B^\sigma]^j \tag{8a}$$

$$= G_B^\sigma + \delta G_L^\sigma + \delta G_R^\sigma + \delta G_{QW}^\sigma, \quad \sigma = \pm. \tag{8b}$$

The second and third terms δG_L^σ and δG_R^σ describe perturbations due to scattering solely on the left or right boundary, respectively, and thus comprise only expressions with V_L^σ or V_R^σ, respectively. The last term δG_{QW}^σ collects all expressions with both V_L^σ and V_R^σ and thus results from multiple scattering between both interfaces, i.e., due to scattering in the quantum well (QW) formed by the two interfaces. The latter may give rise to spin-polarized QW states in the Ni film.[34,35]

If δG_{QW}^σ is neglected, the properties of the film can be regarded as a superposition of perturbations originating from the two independent interfaces. In particular, the magnetization profile of the film $M(l)$—l being the layer index—can be regarded as a superposition of the magnetization profiles originating from the Ni/Cu interface, $M_R(l)$, and from the Ni surface, $M_L(l)$,

$$M(l) \approx M_L(l) + M_R(l) - M_B, \tag{9}$$

where M_B is the magnetic moment of bulk Ni. Since the contribution from the QW term usually gives rise only to small constant shifts of the magnetization profile,[33] the superposition provides a good estimate of the magnetization profiles in films. By definition, quantum-size effects show up as the difference between the superimposed and the true magnetization profile of the film.

The above approximative decomposition is not limited to magnetization profiles. Indeed, the response to additional perturbations can be estimated by a superposition of independent interface perturbations as well. This way we are, for example, able to analyze different contributions to the MAE in films, as will be discussed in the following.

Regarding spin-orbit coupling as a perturbation of the Hamiltonian, the Green function will depend on the magnetization direction, for example perpendicular ($\vec{M}^{(\perp)}$) or parallel ($\vec{M}^{(\parallel)}$) to the interfaces. Further, the spin σ is no longer

a good quantum number. In matrix representation, the resulting Green functions can be written as 2×2 block matrices where each block has the size of the unperturbed GF matrix. We denote the corresponding SOC perturbation operator as $\Theta(\vec{M})$, emphasizing its dependence on the direction of the magnetic moments. The GF of the perturbed Ni film, $G(\vec{M})$, is implicitly given by

$$G(\vec{M})=G+G\Theta(\vec{M})G(\vec{M})=G+\delta G(\vec{M}). \tag{10}$$

The Green function G is diagonal in spin space (no spin-orbit coupling) and constructed from G^{+} and G^{-} of the film with $G^{\pm}_{QW}$ being neglected; cf. Eq. (8b). Here $\delta G(\vec{M})$ is given by the Dyson series

$$\delta G(\vec{M})=G\Theta(\vec{M})G+G\Theta(\vec{M})G\Theta(\vec{M})G+\cdots \tag{11}$$

$$\begin{aligned}&=G_B\Theta(\vec{M})G_B+G_B\Theta(\vec{M})G_B\Theta(\vec{M})G_B+\cdots\\&\quad+\delta G_L\Theta(\vec{M})\,\delta G_L+\delta G_L\Theta(\vec{M})\\&\quad\times\delta G_L\Theta(\vec{M})\,\delta G_L+\cdots+\delta G_R\Theta(\vec{M})\,\delta G_R\\&\quad+\delta G_R\Theta(\vec{M})\,\delta G_R\Theta(\vec{M})\\&\quad\times\delta G_R+\cdots+\delta G_{QW}(\vec{M}).\end{aligned} \tag{12}$$

Eventually, we obtain the grouping of terms

$$\delta G(\vec{M})=\delta G_B(\vec{M})+\delta G_L(\vec{M})+\delta G_R(\vec{M})+\delta G_{QW}(\vec{M}), \tag{13}$$

where $\delta G_L(\vec{M})$ and $\delta G_R(\vec{M})$ include contributions solely from scattering at the left-hand and right-hand side perturbations, respectively. The term $\delta G_B(\vec{M})$ represents the spin-orbit perturbation of bulk Ni, and $\delta G_{QW}(\vec{M})$ includes multiple scattering at both interfaces. If we neglect the latter, the band energy can be expressed as

$$E_{\mathrm{bnd}}(\vec{M})\approx E_{\mathrm{bnd},L}(\vec{M})+E_{\mathrm{bnd},R}(\vec{M})-E_{\mathrm{bnd},B}(\vec{M}), \tag{14}$$

with

$$E_{\mathrm{bnd},B}(\vec{M})=-\frac{1}{\pi}\int_{-\infty}^{E_{\mathrm{F}}}\mathrm{Im\,Tr}\,E\,\delta G_B(\vec{M})\,dE \tag{15}$$

and

$$E_{\mathrm{bnd},D}(\vec{M})=-\frac{1}{\pi}\int_{-\infty}^{E_{\mathrm{F}}}\mathrm{Im\,Tr}\,E[\,\delta G_B(\vec{M})+\delta G_D(\vec{M})\,]dE, \tag{16}$$

where $D=L,R$. According to Eq. (14), this is simply a superposition of three band-energy profiles which result from two independent interfaces on the left- and right-hand sides—$E_{\mathrm{bnd},L}(l)$ and $E_{\mathrm{bnd},R}(l)$—in conjunction with the subtraction of the bulk contribution $E_{\mathrm{bnd},B}$. It provides a picture derived from individual contributions from different kinds of interfaces and surfaces. Again, finite-size effects can be obtained from the difference between the superimposed and the true band energy for the thin film. Considering the band-energy differences $\Delta E_{\mathrm{bnd},D}=E_{\mathrm{bnd},D}(\vec{M}^{(\parallel)})-E_{\mathrm{bnd},D}(\vec{M}^{(\perp)}),D=B,L,R$, only a small number of constituents has to be regarded in order to understand the magnetic anisotropy of layered structures. In analogy with earlier analysis,[36,37] we may thus regard the MAE of thin films as the sum of a surface, an interface part and a bulk contribution if multiple-scattering effects are neglected. However, all three contributions will be of importance and may give rise to a broad spectrum of possible effects on the MAE of thin films.

IV. RESULTS AND DISCUSSION

In this section we discuss the layer-resolved spin moments and the magnetic anisotropy. For the latter we address in particular the effect of lattice relaxations on the band-energy contribution to the MAE and higher-order contributions.

A. Layer-resolved magnetic structure

As is well known, an increase in volume—as well as a reduction of the coordination number—usually favors an increase of the magnetic moment. Thus, the bulk spin magnetic moment of Ni ($0.67\mu_{\mathrm{B}}$) in the fcc case (with Cu lattice constant) is slightly enhanced with respect to that of bulk Ni ($0.62\mu_{\mathrm{B}}$, with Ni lattice constant).[38]

In Fig. 3 the spin magnetization profiles of fcc Ni films on Cu(001) are depicted for coverages from 1 ML up to 10 ML. At 1 ML coverage the magnetic moment is only 44% ($0.296\mu_{\mathrm{B}}$) of the Ni bulk value. For 2 ML the magnetic moments are increased to $0.741\mu_{\mathrm{B}}$ and $0.499\mu_{\mathrm{B}}$ for layers S and $S-1$, respectively. This increase is continued for the 3-ML film. The surface layer of the latter has the largest moment of all systems considered here ($0.762\mu_{\mathrm{B}}$). At 4 ML coverage the building up of a plateau region starts: the interior Ni layers start to show nearly the moments of bulk Ni, while that of the surface layer is enhanced and those at the interface are reduced by about 30% for the first interface Ni layer (adjacent to the first Cu substrate layer, $S-n+1$) and 3% for the second interface Ni layer ($S-n+2$). This ''evolution'' of the magnetization profile is completed at about 7 ML coverage.

The surface magnetic structure of films with $n\geqslant7$ shows a nearly complete agreement with that of semi-infinite Ni(001) ($n=\infty$ in Fig. 3). The magnetic moment of the outermost Ni layer (S, $0.746\mu_{\mathrm{B}}$ for $n=\infty$) compared to those of the interior Ni layers of the film and that of bulk Ni with Cu lattice constant ($0.667\mu_{\mathrm{B}}$) is enhanced by about 12%. This enhancement of moments is typical for surface layers[35] and is due to the reduction in coordination number.

The reduced Ni magnetic moment at the interface can be understood from the behavior of binary bulk alloys $\mathrm{Ni}_x\mathrm{Cu}_{1-x}$ when the concentration x is adjusted to correspond to the Ni-Ni coordination number at the fcc(001) interface.[39] The magnetic properties of binary $3d$ transition-metal alloys are often essentially determined by the nearest-neighbor correlation, i.e., the local environment of a particular atom. The Ni atoms at the Ni/Cu interface can be regarded as constituents of a ''perfectly ordered alloy'' where only 8 of 12 nearest neighbors surrounding an interface Ni site are of the same kind. This corresponds to a local Ni concentration of $x=2/3$. According to the Slater-Pauling curve,[40,41] there is a

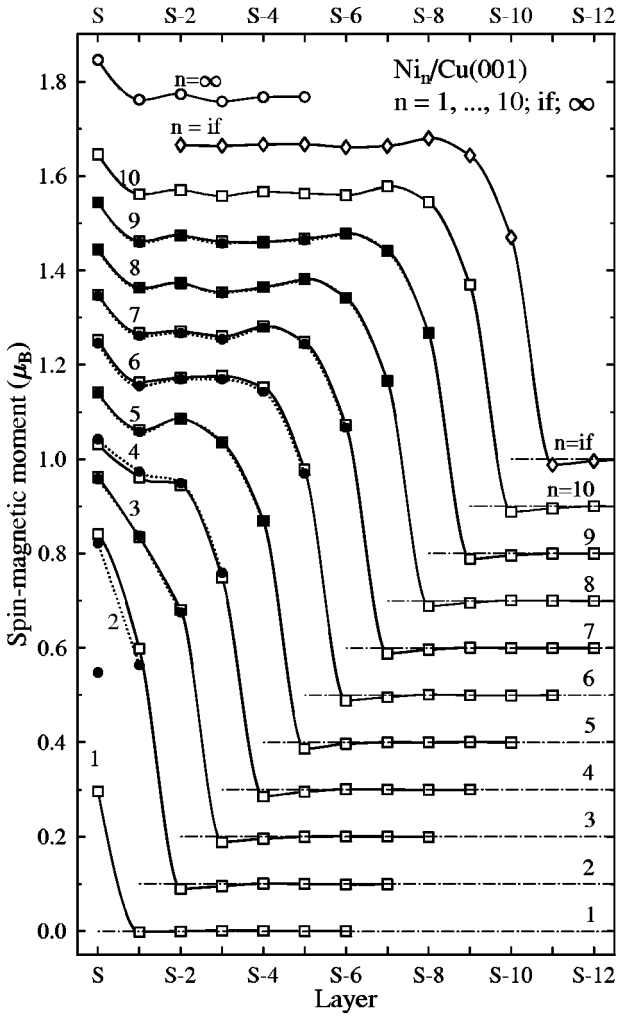

FIG. 3. Layer-resolved spin magnetic moments of fcc Ni films on Cu(001) (squares, solid lines) with thicknesses $n=1,\ldots,10$ as obtained by LMTO calculations. The moments of a Ni(001)/Cu(001) interface [$n=$if, diamonds; interface at layers $S-10$ (Ni) and $S-11$ (Cu)] and semi-infinite Ni(001) ($n=\infty$, open circles)—both with Cu lattice constant—are shown in addition. Magnetic moments obtained by superposition of the surface and the interface profile—cf. Eq. (9)—are indicated by solid circles and dotted lines. For clarity, the data sets are shifted by $0.1(n-1)\mu_B$ ($1.0\mu_B$ for $n=$if, $1.1\mu_B$ for $n=\infty$); their respective zeros are represented by dash-dotted lines. Layers are labeled $S, S-1, S-2, \ldots,$ starting with the surface layer S. Solid and dotted lines serve as guide to the eye.

substantial reduction of the nickel magnetic moment to approximately $0.3\mu_B$ in the Ni_xCu_{1-x} alloy.

The Cu layers next to the interface show induced magnetic moments of about $0.015\mu_B$ with an antiferromagnetic coupling to Ni. For example, this common antiparallel spin behavior has been observed for Fe films on Au(001) by Szunyogh *et al.*[30]

The small oscillations of the size of the magnetic moments in the interior of thicker Ni films ($n>6$) can be regarded as 'magnetic' Friedel oscillations due to the spin-dependent perturbations from the surface and the Ni/Cu interface [they were also found for Co films on Cu(001) (Ref. 37)]. In Fig. 3, both the surface ($n=\infty$) and the interface ($n=if$) system show oscillations which decay rapidly.

We now turn to the picture of the magnetization as a superposition of magnetic profiles [Sec. III, in particular Eq. (9)]. In Fig. 3, the superimposed profiles are compared with their exactly calculated counterparts. Except for the 1-ML film—where the superposition is apparently questionable—we find excellent agreement which means that QW contributions to the spin magnetic moment are generally very small. The largest deviations are found for 2 ML and 4 ML but are smaller than $0.03\mu_B$. As mentioned above, the 3-ML film shows the largest surface magnetic moment. This can easily be explained within the superposition picture: The moment of the surface layer S is obtained from the surface layer S of the surface system and the third Ni layer of the interface system (layer $S-8$ in Fig. 3). Both show the largest moments of their systems and, therefore, give rise to the enhanced surface moment of the 3-ML film. In conclusion, one can construct layer-dependent spin magnetic profiles of films from the surface and the interface profiles with high accuracy, the only exception being the 1-ML case.

Finally, the magnetization profiles shown in Fig. 3 exhibit no spectacular features but rather the expected behavior: enhancement at the surface, reduction at the interface, oscillations in between. Relevant for the discussion of the anisotropy, in particular the band energy, may be the building up of a plateau, i.e., the appearance of bulklike layers, which starts at 6–7 ML.

B. Magnetic anisotropy

The magnetic-anisotropy energy is composed of two parts, the dipole-dipole interaction energy $\Delta E_{dd}=E_{dd}(\vec{M}^{(\|)})-E_{dd}(\vec{M}^{(\perp)})$ and the band-energy contribution $\Delta E_{bnd}=E_{bnd}(\vec{M}^{(\|)})-E_{bnd}(\vec{M}^{(\perp)})$, Eq. (7). The former is negative for all thicknesses, thus favoring in-plane anisotropy, and depends almost linearly on film thickness. Therefore, the first spin reorientation transition can exclusively be attributed to the band-energy part which is discussed in the following by means of the layer-resolved band-energy difference $\Delta E_{bnd}^{(l)}=E_{bnd}^{(l)}(\vec{M}^{(\|)})-E_{bnd}^{(l)}(\vec{M}^{(\perp)})$, with l denoting the layer.

We first address films with fcc structure (fcc case, solid lines in Fig. 4). An interface between Ni(001) and Cu(001) favors an in-plane orientation of the magnetic moments ($\Delta E_{bnd}=-65\ \mu\text{eV}<0$), as is evident from the "$n=$if" curve in Fig. 4. Here, the last Ni layer is $S-9$, and the first Cu layer is $S-10$. Further, there are oscillations within the Ni half-space with a wavelength of approximately five layers. The surface of semi-infinite Ni(001) ("$n=\infty$" curve in Fig. 4) also favors in-plane anisotropy ($\Delta E_{bnd}=-43\ \mu$eV). Remarkably, the second and third outermost layers $S-1$ and $S-2$ appear to have a rather large positive band-energy difference which, however, is overridden by the subsequent layers. Regarding only the first three outermost layers, $\Delta E_{bnd}=22\ \mu$eV. The most significant layers, i.e., those layers which show the largest absolute value of band-energy difference, are the first outermost four layers in the case of semi-infinite Ni(001) and the nearest and second-nearest Ni layers to the Ni/Cu interface.

The layer-resolved band-energy difference of the 10-ML film can be regarded as composed by the interface and the surface profiles. This is evident by comparing its profile ob-

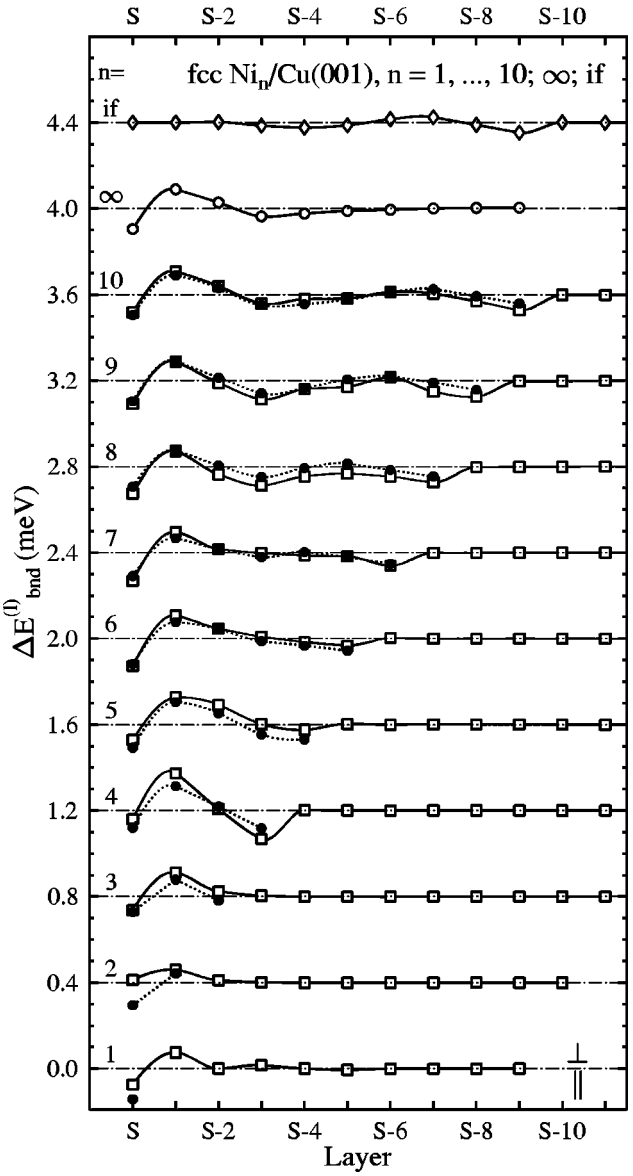

FIG. 4. Layer-resolved band-energy contribution to the magnetic-anisotropy energy of fcc Ni films (fcc case) on Cu(001) with thicknesses $n=1,\ldots,10$ (squares), ∞ (open circles), and a Ni/Cu interface at layer $S-9$ (diamonds, ''if''). Solid circles connected by dotted lines refer to band-energy differences obtain by superposition of the surface ($n=\infty$) and the interface ($n=$if) contribution [cf. Eq. (14)]. For clarity, the data sets are shifted by $0.4(n-1)$ meV (4.0 meV for $n=\infty$, 4.4 meV for ''if''); their respective zeros are represented by dash-dotted lines. Layers are labeled S, $S-1$, $S-2,\ldots$, starting with the surface layer S. Solid and dotted lines serve as guide to the eye.

tained from the LKKR calculations with that obtained from a superposition of the latter profiles using Eq. (14). We find this agreement also for film thicknesses of 6 ML, 7 ML, and 9 ML. The composed profile of the 8-ML film shows slightly too high values; the shape of the profile, however, is nicely reproduced. In conclusion, the superposition of profiles works well at higher film thicknesses, meaning that the QW part of the band-energy difference is small. Further, this corresponds nicely with the onset of bulklike magnetization profiles (Sec. IV A) which we observed in the interior of thick films ($n\geqslant 6$).

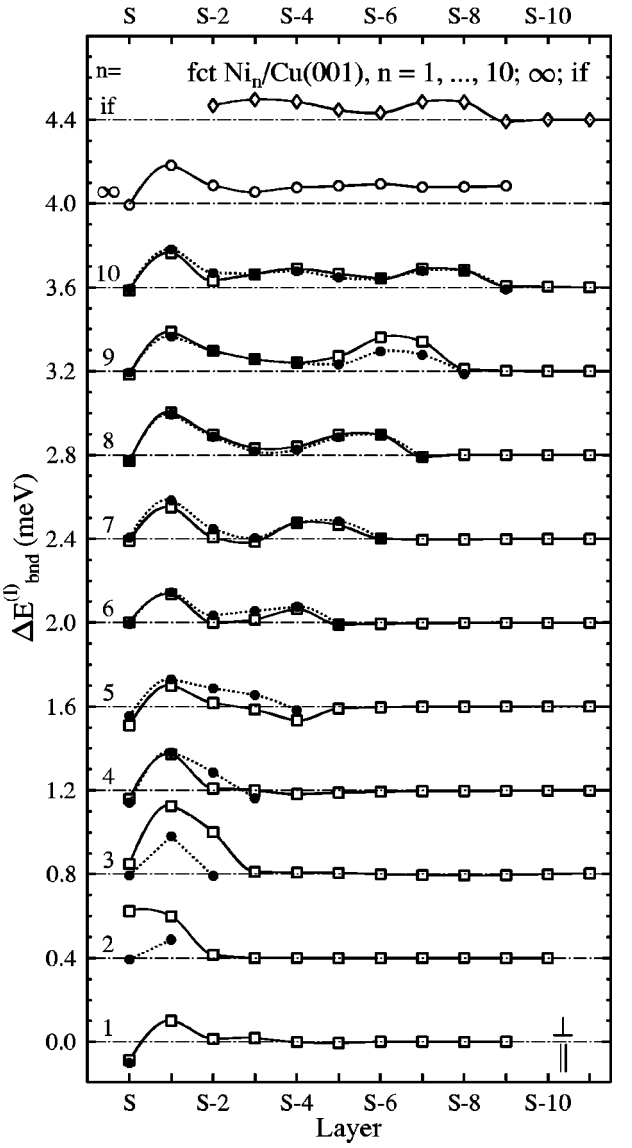

FIG. 5. Same as Fig. 4, but for tetragonally distorted Ni films (fct case).

For small film thicknesses, 1–5 ML, the above-mentioned significant ranges of layers of semi-infinite Ni and the Ni/Cu interface overlap in the superposition picture. From 3 ML to 5 ML, the superposition yields the correct shapes of the profiles and also correct signs of the values, but mostly gives too small absolute values compared to those of the full calculation. For 1 ML and 2 ML, the value for the layer S is overestimated in absolute value. Further, the sign is wrong in the case of 2 ML. We regard these deviations as manifestations of the QW part of the band-energy difference.

In the whole range of film thicknesses, except for 1 ML, we find no significant contribution to ΔE_{bnd} from the Cu layers. For the 1-ML film, however, the Cu layer $S-1$ shows a considerable positive band-energy difference, although the layer shows only a very small magnetic moment (compared to that of the Ni layer S). This finding emphasizes that there is no simple relation between magnetic moment and band-energy difference. Note that the latter is the first energy moment of the former [cf. Eq. (3)].

We now focus on films with fct structure (fct case), the tetragonal distortion of which leads to an uniaxial system.

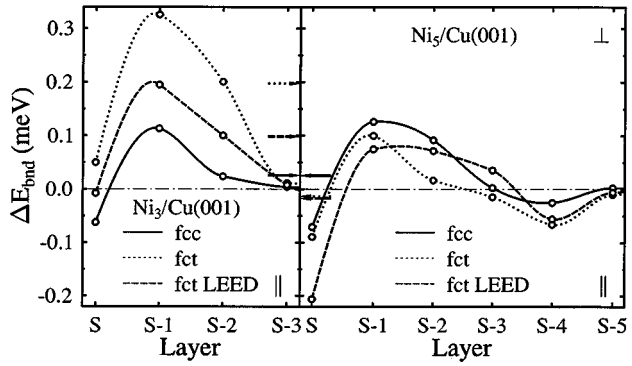

FIG. 6. Layer-resolved band-energy contribution to the magnetic-anisotropy energy of Ni films on Cu(001) with thicknesses $n=3$ (left) and $n=5$ (right) for cubic (solid lines, fcc), homogeneously tetragonal distorted (dotted lines, fct), and inhomogeneously tetragonal distorted (dashed lines, fct LEED) systems. Arrows mark averages over the Ni layers. The layers are labelled $S, S-1, S-2, \ldots$, starting with the surface layer S. Lines serve as guide to the eye.

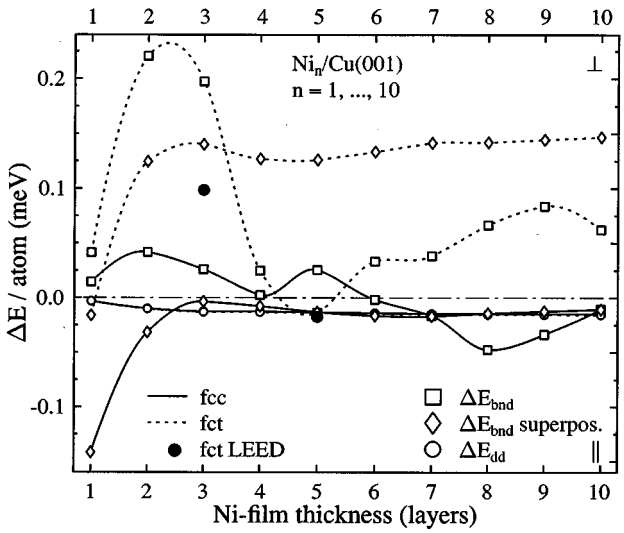

FIG. 7. Magnetic-anisotropy energies per atom of Ni films on Cu(001). Their band-energy contributions ΔE_{bnd} are represented by squares, their dipole-dipole interaction energy ΔE_{dd} by open circles. Diamonds denote band-energy contributions obtained by superposition of the surface and the interface profiles; cf. Eq. (14). Solid lines refer to cubic Ni films (fcc case), dotted lines to homogeneously tetragonal distorted Ni films (fct case). Solid circles show band-energy data obtained for in-homogeneously tetragonal distorted Ni films of 3 ML and 5 ML thickness (fct LEED case). Lines serve as guide to the eye.

For bulklike layers we find a volume contribution (K_v) of 0.081 meV/atom which corresponds nicely with theoretical and experimental results.[15] At first glance, the band-energy difference profile of the Ni/Cu interface (cf. ''$n=$if'' in Fig. 5) appears to be just shifted to positive values but also the wavelength of the oscillations has decreased to approximately four layers. Also the profile of semi-infinite Ni(001) can be regarded as shifted by the volume contribution; its shape remains nearly unchanged. Evidently, both the surface and the interface system clearly favor perpendicular anisotropy ($\Delta E_{\mathrm{bnd}}>0$) due to the tetragonal distortion. If the superposition of profiles works as well as in the fcc case, we expect that films with larger film thickness will also show perpendicular anisotropy.

The overall enhancement of $\Delta E_{\mathrm{bnd}}^{(l)}$ is clearly visible for films with $n\geqslant 6$ (cf. Fig. 5). For example, both the surface layers S and the interface layer $S-n+1$ show values around zero, in the fcc case negative values, though. The profiles are again well reproduced by the superposition, an exception being layers $S-6$ and $S-7$ for $n=9$. For thinner films, the shape of the profiles is not as well reproduced by the superposition as for the thicker films, (cf. in particular $n=2$ and $n=3$), which means that QW contributions are important. Thus, a shift in $\Delta E_{\mathrm{bnd}}^{(l)}$ due to the tetragonal distortion is hard to detect because it might be covered by the QW contribution. So the origin of the significant shift for 2 ML and 3 ML, compared to the fcc case, cannot be unambiguously determined.

For the 3-ML and 5-ML films we now discuss the effect of the tetragonal distortion on the band-energy difference in more detail. In Fig. 6 the layer-resolved band energies for the fcc, fct, and fct LEED cases are shown. As the fct LEED case can be regarded as an intermediate case between the fcc and fct cases, one would expect that its band-energy profile lies between those of the latter. For the 3-ML film this is apparently true (left panel in Fig. 6). The interlayer distances in the fct LEED case[31] are reduced by about 2.6% with respect to that of bulk Cu. So one would be led to the conclusion that—despite possible QW contributions—the result of Fig. 6 is consistent with a volume contribution to the MAE.

For the 5-ML film, however, we observe a completely different dependence on the relaxation (right panel in Fig. 6). Here, the average contraction is 3.8%, but with an outward relaxation of the surface layer by 1.7%. This outward relaxation could explain that the band-energy difference for this layer is the lowest of all three cases. Further, the fcc profile is larger than the fct case for all layers, but the fct LEED profile shows the smallest (layer S) as well as the largest values (layers $S-3$). Considering the averaged band-energy differences (ΔE_{bnd}, arrows in Fig. 6), both fct cases show negative values, i.e., favor in-plane anisotropy. In conclusion, we find no simple relation between relaxation and band-energy contribution to the magnetic anisotropy for thin films.

We now turn to the magnetic-anisotropy energy. The total band-energy difference per Ni atom, Eq. (4), together with the dipole-dipole interaction energy per Ni atom is shown in Fig. 7. For the latter (open circles in Fig. 7), the tetragonal distortion leads to a slightly stronger interaction of the local magnetic moments and thus to an insignificant lower ΔE_{dd}/atom. As mentioned earlier, ΔE_{dd} shows negative values throughout the whole thickness range and depends almost linearly on film thickness. Therefore, ΔE_{dd}/atom is nearly independent on the film thickness for films thicker than three layers. Thus, as was mentioned before, the band-energy contribution to the MAE must be considered as responsible for the first spin reorientation transition.

In the fcc case, ΔE_{bnd}/atom (squares connected by solid lines in Fig. 7) is positive for films with $n\leqslant 5$ and negative otherwise. Summing up both contributions yields perpendicular anisotropy for film thicknesses $n=1$, 2, 3, and 5.

Thus, it completely fails to reproduce the experimental finding of in-plane anisotropy for thin films ($n \leqslant 5$) and perpendicular anisotropy for thicker films ($n \geqslant 6$). However, in the fct case (squares connected by dotted lines in Fig. 7) we observe a volume contribution to the band energy for thicker films. This gives rise to an almost linear increase of ΔE_{bnd} with film thickness for $n \geqslant 6$. It overrides ΔE_{dd} and therefore yields perpendicular anisotropy. For thin films, in particular the 2-ML and 3-ML films, we observe also a strong positive band-energy contribution which results in perpendicular anisotropy. We recall that the fct case by far overestimates the tetragonal distortion. So the fct LEED case is more appropriate (solid circles in Fig. 7) but leads also to perpendicular anisotropy for the 3-ML film. (To our knowledge, LEED investigations for all relevant film thicknesses have not been published up to date.) We would like to note that other calculations[42,43] also show perpendicular anisotropy for 2 ML and 3 ML films with band-energy differences of comparable size. This corroborates that—at least—the thinner films are idealizations of the experimental ones. In experiment, in-plane anisotropy is observed for thin films, but one should keep in mind that experimental samples are not as ''ideal'' as those in a zero-temperature theory due to, e.g., interface roughness, vacancies, and impurities, all of which lower the MAE.[15] Recent experiments[44] show that the quality of Ni films on Cu(001) indeed increases with film thickness. We have therefore performed simple test calculations within the virtual crystal approximation and the averaged *t*-matrix approximation in order to investigate the effect of interface roughness. For thicker films, the effect on the MAE is very small, but for thin films we observe a strong decrease of the MAE or even in-plane anisotropy. These calculations fully confirm the expectations, but we are aware that they can only reveal trends. More sophisticated calculations are therefore needed and are currently in progress.

The band-energy difference ΔE_{bnd}/atom obtained by superposition [diamonds in Fig. 7, Eq. (14)] show identical general shapes in both the fcc and fct cases: at very thin films (one and two layers) there is a strong increase whereas for thicker films ($n \geqslant 3$) the energies are nearly independent on the film thickness. Due to the volume contribution to the MAE, the latter curve is shifted to higher energies. This results in perpendicular anisotropy for film thicknesses $n \geqslant 2$ in the fct case, but in-plane anisotropy for all thicknesses in the fcc case. Thus, the latter fails completely to reproduce the experimental observed spin reorientation transition. The former, however, is able to reproduce the experimentally observed trends correctly but fails to reproduce the SRT film thickness. Quantum-size effects show up in the deviation of band-energy contributions obtained by the full calculation and the superposition of the surface and the interface profile (squares and diamonds in Fig. 7, respectively). In both the fcc and fct cases, quantum-well contributions to the band-energy contribution are strong and influence the anisotropy considerably.

In conclusion, we observe a strong perpendicular anisotropy from 6 ML and beyond which corresponds well with the experimental findings of the first SRT. The interior part of the film—roughly speaking the volume contribution to the MAE—can be regarded as responsible for the first SRT. However, quantum-well contributions to the MAE are strong and effect the film thickness at which the first SRT will occur. In particular, very thin fct films (e.g., 2 ML and 3 ML) show perpendicular anisotropy—in contrast to experiment—which indicates differences between the experimental films and the idealized films in theory. Our calculations show that the correct geometry (as, for example, obtained by LEED) as well as film imperfections have to be included in future work in order to explain this disagreement. To conclude on the second SRT (transition from perpendicular to in-plane magnetic moments which occurs around 35–70 ML) is difficult due to strain relaxation in thick films and island growth in experiment.[3,4,16]

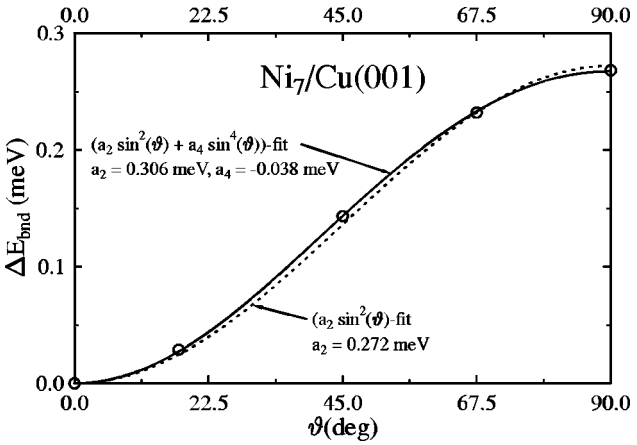

FIG. 8. Higher-order contribution to the band-energy difference ΔE_{bnd} of 7 ML fct Ni on Cu(001). ϑ is the polar tilt angle of the magnetic moments [cf. Eq. (17)]. Circles represent results of the numerical calculations. The dotted line is a fit taking into account only the first-order contribution (a_2); the solid line is a fit for both first- and second-order contributions (a_2 and a_4).

At last, we address higher-order contributions to the MAE. For the film thickness of 7 ML in the fct case, the band-energy difference ΔE_{bnd} was calculated for magnetic moments tilted at an polar angle ϑ: $\vec{M}(\vartheta) = \vec{M}^{(\perp)} \cos\vartheta + \vec{M}^{(\parallel)} \sin\vartheta$. The dipole-dipole interaction energy is proportional to $\sin^2\vartheta$.[37] For the band energy we make the ansatz

$$E_{\mathrm{bnd}}(\vartheta) = a_2 \sin^2\vartheta + a_4 \sin^4\vartheta \tag{17}$$

and determined the coefficients a_2 and a_4 by least-squares fitting to the numerical results; cf. Fig. 8. The dotted line in Fig. 8 is the best fit when setting $a_4 = 0$, i.e., taking into account only the first-order contribution ($a_2 = 0.272$ meV). Apparently, it deviates visibly from the numerically obtained data. Taking into account the second-order contribution we find a perfect fit ($a_2 = 0.306$ meV, $a_4 = -0.038$ meV). As in experiment, the first-order contribution is positive while the second-order contribution is negative.[14] To compare the theoretical anisotropy constants (obtained in a zero-temperature model) with experimental ones is difficult because they depend significantly on temperature (cf. Fig. 6 in Ref. 45). Thus, experimental values should be extrapolated to zero temperature which is—at present—hardly possible. At a reduced temperature $T/T_C = 0.2$ Baberschke and Farle[45] found for 7–8-ML films $a_2 \approx 0.101$ meV and $a_4 \approx -0.019$ meV. Thus, theory gives values approximately a factor of 2–3 too high which—besides the finite

temperature—can be attributed to sample imperfections in experiment (which lower the MAE) or an overestimation of the lattice relaxation in theory (which increases the MAE).

Having focused on the film-averaged anisotropy constants, we now address briefly the layer-resolved values of a_2 and a_4. A closer analysis reveals that a_2 follows the band-energy difference profile very closely (cf. Fig. 5); in other words the first-order contribution is dominant for all layers. a_4 is negative for all Ni layers except for layer $S-1$ where it is positive but very small (<0.0005 meV). Multiplied by a factor, it agrees surprisingly nicely with the band-energy difference profile but appears to be shifted down in energy. The largest deviations are at layers S, $S-5$, and $S-6$, i.e., at the surface and at the interface. Further, a_2 and a_4 show the same sign for layers S, $S-1$, and $S-3$. As a rule of thumb, the layer-dependent first-order contribution a_2 can in good approximation be taken from the band-energy difference profiles, the second-order contribution a_4 as layer-independent and negative for all layers.

V. CONCLUDING REMARKS

Film geometry, i.e., tetragonal distortion, and magnetic properties, in particular the anisotropy, of ultrathin Ni layers on Cu(001), are closely related. We have calculated both magnetization profiles and magnetic anisotropy of cubic and tetragonally distorted films for thicknesses from 1 ML up to 10 ML.

Thick fct films (with thicknesses larger than five monolayers) show an increase of the volume contribution to the magnetic-anisotropy energy which overrides the dipole-dipole interaction contribution. Thus, the experimentally observed spin reorientation transition from in-plane to perpendicular anisotropy at around six monolayers Ni can be attributed to this volume contribution. The surface anisotropy, i.e., perpendicular anisotropy at the outermost two to three layers, is too small compared to the volume contribution and thus cannot account for the observed transition. Further, the interface contribution favors an in-plane anisotropy which partially cancels the surface anisotropy.

In thin fct films (with thicknesses less than 6 ML) effects due to the quantization of electronic states within the Ni film are found to be significant. For these, we observe also perpendicular anisotropy, in particular for 2 ML and 3 ML thickness. This is in contrast to experiments but in agreement with other calculations[42,43] and, thus, gives evidence that idealized theoretical systems do not fully describe the experimental situation. Especially, mechanisms which lower the band-energy contribution to the MAE—such as surface and interface roughness[44]—are yet not taken into account. Simple test calculations for the effect of interface roughness yield a decrease of the MAE—as expected—but should be followed by more advanced work.

ACKNOWLEDGMENTS

We very much appreciate fruitful discussions with K. Baberschke (Berlin) and H. L. Skriver (Lyngby). This work has been performed within the Training and Mobility of Researchers (TMR) Network ''Interface Magnetism.'' We also thank the Swedish Natural Science Research Council (NFR) and the Swedish Materials Consortium No. 9 financed by NUTEK and NFR for valuable support.

[1] B. Schulz and K. Baberschke, Phys. Rev. B **50**, 13 467 (1994).
[2] B. Schulz, R. Schwarzwald, and K. Baberschke, Surf. Sci. **307-309**, 1102 (1994).
[3] W. L. O'Brien and B. P. Tonner, J. Appl. Phys. **79**, 5623 (1996).
[4] W. L. O'Brien, T. Droubay, and B. P. Tonner, Phys. Rev. B **54**, 9297 (1996).
[5] J. Hunter Dunn, D. Arvinitis, and N. Mårtensson, Phys. Rev. B **54**, R11 157 (1996).
[6] R. Lorenz and J. Hafner, Phys. Rev. B **54**, 15 937 (1996).
[7] B. Újfalussy, L. Szunyogh, and P. Weinberger, Phys. Rev. B **54**, 9883 (1996).
[8] M. Zharnikov, A. Dittschar, W. Kuch, C. M. Schneider, and J. Kirschner, J. Magn. Magn. Mater. **174**, 40 (1997).
[9] A. Berger, B. Feldmann, H. Zillgen, and M. Wuttig, J. Magn. Magn. Mater. **183**, 35 (1998).
[10] C. M. Schneider, Ph.D. thesis, Freie Universität Berlin, 1990.
[11] W. Weber, A. Bischof, R. Allenspach, C. Back, J. Fassbender, U. May, B. Schirmer, R. Jungblut, G. Güntherodt, and B. Hillebrands, Phys. Rev. B **54**, 4075 (1996).
[12] Q. Y. Jin, H. Regensburger, R. Vollmer, and J. Kirschner, Phys. Rev. Lett. **80**, 4056 (1998).
[13] A. B. Shick, D. L. Novikov, and A. J. Freeman, J. Magn. Magn. Mater. **177-181**, 1223 (1998).
[14] M. Farle, B. Mirwald-Schulz, A. N. Anisimov, W. Platow, and K. Baberschke, Phys. Rev. B **55**, 3708 (1997).
[15] O. Hjortstam, K. Baberschke, J. M. Wills, B. Johansson, and O. Eriksson, Phys. Rev. B **55**, 15 026 (1997).
[16] J. Shen, J. Giergiel, and J. Kirschner, Phys. Rev. B **52**, 8454 (1995).
[17] O. K. Andersen, Phys. Rev. B **12**, 3060 (1975).
[18] H. Skriver, *The LMTO-Method* (Springer, Berlin, 1984).
[19] H. L. Skriver and N. M. Rosengaard, Phys. Rev. B **43**, 9538 (1991).
[20] O. K. Andersen and O. Jepsen, Phys. Rev. Lett. **53**, 2571 (1984).
[21] S. H. Vosko, L. Wilk, and M. Nusair, Can. J. Phys. **58**, 1200 (1980).
[22] B. Wenzien, J. Kudrnovský, V. Drchal, and M. Šob, J. Phys.: Condens. Matter **1**, 9893 (1989).
[23] E. Tamura, in *Applications of Multiple Scattering Theory to Materials Science*, edited by W. H. Butler, P. H. Dederichs, A. Gonis, and R. L. Weaver, MRS Symposia Proceedings No. 253 (Materials Research Society, Pittsburgh, 1992), p. 347.
[24] *Electron Scattering Theory of Ordered and Disordered Matter*, edited by P. Weinberger (Clarendon Press, Oxford, 1990).
[25] H. J. Monkhorst and J. D. Pack, Phys. Rev. B **13**, 5188 (1976).
[26] R. Evarestov and V. Smirnow, Phys. Status Solidi B **119**, 9 (1983).
[27] S. S. A. Razee, J. B. Staunton, and F. J. Pinski, Phys. Rev. B **56**, 8082 (1997).
[28] S. V. Halilov, A. Y. Perlov, P. M. Openeer, A. N. Yaresko, and

V. N. Antonov, Phys. Rev. B **57**, 9557 (1998).
[29] *Handbook of Mathematical Functions*, edited by M. Abramowitz and I. Stegun (Dover, New York, 1970).
[30] L. Szunyogh, B. Újfalussy, and P. Weinberger, Phys. Rev. B **51**, 9552 (1995).
[31] S. Müller, B. Schulz, G. Kostka, M. Farle, K. Heinz, and K. Baberschke, Surf. Sci. **364**, 235 (1996).
[32] S. Müller, A. Kinne, M. Kottke, R. Metzler, P. Bayer, L. Hammer, and K. Heinz, Phys. Rev. Lett. **75**, 2859 (1995).
[33] A. M. N. Niklasson, S. Mirbt, H. L. Skriver, and B. Johansson, Phys. Rev. B **53**, 8509 (1996).
[34] J. E. Ortega, F. J. Himpsel, G. J. Mankey, and R. F. Willis, Phys. Rev. B **47**, 1540 (1993).
[35] F. J. Himpsel, J. E. Ortega, G. J. Mankey, and R. F. Willis, Adv. Phys. **47**, 511 (1998).
[36] B. Heinrich and J. F. Cochran, Adv. Phys. **42**, 523 (1993).
[37] L. Szunyogh, B. Újfalussy, C. Blaas, U. Pustogowa, C. Sommers, and P. Weinberger, Phys. Rev. B **56**, 14 036 (1997).
[38] K. Baberschke, Appl. Phys. A: Mater. Sci. Process. **62**, 427 (1996).
[39] A. M. N. Niklasson, B. Johansson, and H. L. Skriver, Phys. Rev. B **59**, 6373 (1999).
[40] K. Adachi, D. Bonnenberg, K. A. Hempel, and H. P. J. Wijn, in *Magnetic Properties of Metals*, edited by H. P. J. Wijn, Landolt-Börnstein, New Series, Group 3, Vol. 19, Pt. a (Springer, Berlin, 1986), Chap. 1.2, p 142.
[41] P. James, O. Eriksson, B. Johansson, and I. A. Abrikosov, Phys. Rev. B **59**, 419 (1999).
[42] C. Uiberacker, J. Zabloudil, P. Weinberger, L. Szunyogh, and C. Sommers, Phys. Rev. Lett. **82**, 1289 (1999).
[43] D. Spišák and J. Hafner (unpublished).
[44] W. Platow, A. N. Anisimov, G. L. Dunifer, M. Farle, and K. Baberschke, Phys. Rev. B **58**, 5611 (1998).
[45] K. Baberschke and M. Farle, J. Appl. Phys. **81**, 5038 (1997).